NANO LETTERS

2008
Vol. 8, No. 11
3766-3770

Terahertz Near-Field Nanoscopy of Mobile Carriers in Single Semiconductor Nanodevices

A. J. Huber,[†,‡] F. Keilmann,[†] J. Wittborn,[§] J. Aizpurua,[||] and R. Hillenbrand*[,†,‡]

Max-Planck-Institut für Biochemie and Center for NanoScience, 82152 Martinsried (München), Germany, CIC nanoGUNE, 20009 Donostia − San Sebastian, Spain, Infineon Technologies AG, 81739 München, Germany, and Donostia International Physics Center (DIPC) and Centro Mixto de Fisica de Materiales (CSIC-UPV/EHU), 20018 Donostia − San Sebastian, Spain

Received July 15, 2008

ABSTRACT

We introduce ultraresolving terahertz (THz) near-field microscopy based on THz scattering at atomic force microscope tips. Nanoscale resolution is achieved by THz field confinement at the very tip apex to within 30 nm, which is in good agreement with full electro-dynamic calculations. Imaging semiconductor transistors, we provide first evidence of 40 nm (λ/3000) spatial resolution at 2.54 THz (wavelength $\lambda = 118$ μm) and demonstrate the simultaneous THz recognition of materials and mobile carriers in a single nanodevice. Fundamentally important, we find that the mobile carrier contrast can be directly related to near-field excitation of THz-plasmons in the doped semiconductor regions. This opens the door to quantitative studies of local carrier concentration and mobility at the nanometer scale. The THz near-field response is extraordinary sensitive, providing contrast from less than 100 mobile electrons in the probed volume. Future improvements could allow for THz characterization of even single electrons or biomolecules.

Electromagnetic radiation at THz frequencies addresses a rich variety of light-matter interactions because photons in this low energy range can excite molecular vibrations and phonons, as well as plasmons and electrons of nonmetallic conductors.[1−4] Consequently, THz radiation offers intriguing possibilities for material and device characterization currently motivating major efforts in the development of THz imaging systems.[5,6] Diffraction unfortunately limits the spatial resolution to about half the wavelength which is in the order of about 100 μm. For this reason, THz mapping of micro- or nanoelectronic devices, low-dimensional semiconductor nanostructures, cellular entities or single molecules could not be attained. A promising route to break the diffraction barrier and to enable subwavelength scale imaging is based on fine-focusing of THz radiation by millimeter-long tapered metal wires.[7−10] Acting as antennas, the wires capture incident THz waves and convert them into strongly confined near fields at the wire tip apex.[11] When this confined field becomes modified by a close-by scanned sample, the scattered radiation carries information on the local dielectric properties of the sample.[9,12,13] THz images can be obtained by recording the scattered radiation by a distant THz receiver. Attempts of realizing such THz-scattering near-field optical microscopy (THz-SNOM), however suffer from weak signals and faint material contrasts owing to strong background scattering. Novel probes for THz focusing are thus a subject of current interest[14,15] but nanoscale resolved imaging has not yet been demonstrated.

Here we introduce and demonstrate THz near-field microscopy that achieves unprecedented resolution of about 40 nm, paired with extraordinarily high image contrast and acquisition speed. This is enabled by interferometric detection of THz radiation scattered from cantilevered atomic-force-microscope (AFM) tips. Studying a test sample and semiconductor transistors, we provide fundamental insights into THz near-field interactions at the nanometer scale and demonstrate plasmon-assisted THz mapping of mobile carriers within a single nanodevice.

The essential ingredient to nanoscale resolved THz near-field microscopy is a strongly confined THz near field for generating highly localized scattering. As we predict in Figure 1a, nanoscale near-field confinement can be achieved by plane-wave illumination of a conical metal tip, similar to visible[16] and infrared[17] frequencies. The numerically calcu-

* To whom correspondence should be addressed. E-mail: hillenbr@biochem.mpg.de.
[†] Max-Planck-Institut für Biochemie and Center for NanoScience.
[‡] CIC nanoGUNE.
[§] Infineon Technologies AG.
[||] Donostia International Physics Center (DIPC) and Centro Mixto de Fisica de Materiales (CSIC-UPV/EHU).

10.1021/nl802086x CCC: $40.75
Published on Web 10/07/2008

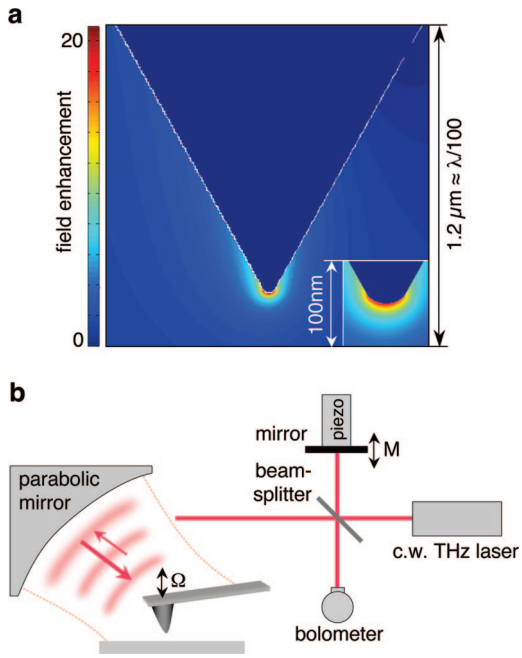

Figure 1. THz near-field microscopy based on field concentration at sharp metal tips. (a) The calculated field distribution at the tip apex of a metal cone with length $L = 1.0\ \mu$m shows nanoscale field confinement and 25-fold field enhancement at the tip apex. (b) Scheme of our experimental setup based on a tapping-mode AFM: a laser emitting a monochromatic beam at 2.54 THz is used for illuminating a cantilevered AFM tip and interferometric detection is used for recording the backscattered THz radiation simultaneously with the AFM topography.

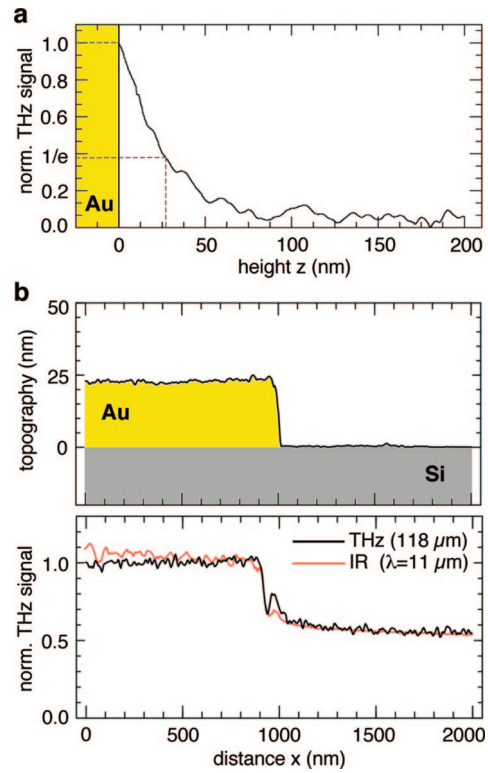

Figure 2. (a) Experimental demonstration of nanoscale THz near-field confinement: the THz signal s_3 recorded vs tip height z over an extended Au surface decreases rapidly with z. (b) Demonstration of near-field THz contrast by scanning a partly Au covered Si test sample. Topography (top) and THz signal s_3 (bottom, black curve) are recorded simultaneously. The THz signal exhibits a clear, strong material contrast between Au and Si. For comparison, we show a repeat of the same line scan, obtained with the same tip but with mid-infrared illumination at 28 THz from a CO_2 laser (red curve).

lated field distribution at the apex (curvature radius $r = 30$ nm) of an even short metal tip with length $L = 1\ \mu$m clearly shows field confinement to about 30 nm in all three directions. This result was obtained for 2.54 THz radiation ($\lambda = 118\ \mu$m) incident at 60° from the tip axis. The full electrodynamical calculations were performed by using the boundary element method (BEM) to exactly solve Maxwell's equations for this configuration.[18,19] We consider finite values for the real and imaginary parts of the dielectric response of the metallic tip, consistent with a Drude-like behavior in this spectral range. The strong confinement as well as an about 25-fold field enhancement (compared to the incident field) are essentially caused by the lightning-rod effect.[20] We note that because of the short tip length ($L \ll \lambda$), geometrical antenna resonances[7,14] can be neglected. Also, dielectric plasmon resonances of a metal tip are absent at THz frequencies.

Experimentally we realize nanoscale-confined THz near fields by means of cantilevered Si tips ($L \approx 20\ \mu$m) with a Pt metallization of about 20 nm thickness (Mod. CSC37/Ti−Pt, Mikromasch). While the sample is scanned in conventional AFM tapping mode, both the tip (with curvature radius of about 30 nm) and the cantilever are illuminated with a focused laser beam at a frequency of 2.54 THz from a continuous-wave CH_3OH gas laser (Mod. SIFIR-50, Coherent) at a power of about 5 mW (Figure 1b). THz imaging is performed by collecting the back-scattered radiation with a parabolic mirror. For detection we use a Michelson interferometer featuring a 23 μm thick polyethylene beam splitter at 45° incidence. Interferometric detection offers the advantage of signal amplification which is crucial for measuring the back-scattered THz radiation with a high signal-to-noise ratio at reasonable integration times less than 100 ms per pixel. As THz detector, we use a hot-electron bolometer (Mod. RS1−5T, Scontel). In order to eliminate background scattering, the AFM is operated in dynamic mode where the cantilever oscillates at its mechanical resonance frequency Ω, here at 35 kHz, with an amplitude of about 100 nm_{pp}. The bolometer signal is subsequently demodulated at harmonic frequencies $n\Omega$ (with $n = 2$ or 3) yielding a background-free THz signal amplitude s_n.[12,21]

To validate THz near-field confinement at the metallized AFM tip, we perform near-field measurements on a well-defined test sample, a 23 nm thick structured Au film deposited on a Si substrate. In a first experiment, we recorded the THz amplitude signal s_3 as a function of the distance z between the tip and the Au surface (approach curve, Figure 2a). We find that s_3 rapidly decays when z increases. At $z \approx 30$ nm, the signal is already reduced by a factor 1/e. This observation clearly demonstrates the nanoscale localization of the tip−sample near-field interaction in z-direction to about $\lambda/4000$, which is consistent with the calculated field confinement shown in Figure 1a. At distances $z > 50$ nm, the THz signal approaches the noise level of

the detector, verifying full suppression of background scattering.

A second experiment with our test sample validates the near-field THz contrast between different materials. We scanned a sample area where the Au film was partly removed and recorded topography (height) and THz signal s_3 simultaneously (Figure 2b, black curve). We observe distinct THz signal levels for Au and Si, and take the transition width <150 nm as an upper bound for the achieved spatial resolution. The dielectric material contrast is orders of magnitude stronger than previously reported,[9,10,22] amounting to $s_3(\mathrm{Si})/s_3(\mathrm{Au}) = 0.55$, which is nearly equal to observations with scattering-type near-field microscopy at mid-infrared (IR) frequencies.[12,23] To quantify this phenomenon in direct comparison, we repeated the scan of the sample with the same tip but with CO_2 laser illumination at 28 THz ($\lambda \approx 11$ μm). Interestingly, a nearly identical contrast profile (red curve in Figure 2b) is observed, indicating the common nature of the near-field optical contrast mechanisms at IR and THz frequencies. We note that the infrared contrast can be well explained by dipolar coupling between tip and sample where the tip polarizability is considered to correspond to that of a metallic sphere.[12] This model predicts that the contrast between Au and Si is the same at both IR and THz frequencies, confirming our experimental data. Hence we conclude that dipolar near-field coupling between a metallic tip and a sample can well describe the relative material contrast in THz near-field microscopy even though the metallic tip has a finite length. For calculating the absolute levels of scattering signals, of course, an improved theoretical description is needed which takes account of the real geometry of the tip and possible antenna effects. Nevertheless, our fundamental finding of a wavelength-independent contrast mechanism is the key to ultrabroadband optical near-field microscopy as spectroscopic image contrasts can be directly related to dielectric sample properties.

By imaging a polished cut through nanoscale transistor structures, we demonstrate the simultaneous recognition of materials and mobile carriers by THz near-field microscopy. While the AFM topography (Figure 3a, gray) only shows some depressions where metal contacts (Cu, W) were differently polished than SiO_2, the THz image (Figure 3a, color) clearly recognizes seven transistors manufactured in Si with polycrystalline Si gates and with SiO_2 as insulating material. The THz contrast can be clearly related to the different materials composing the transistors as we verify by scanning electron microscopy (SEM) of a similar sample where decoration etching was employed to highlight the different materials (Figure 3b). We find that regions with metals or highly conductive semiconductors appear brightest in the THz image, the lowly doped semiconductors darker, and the low-refractive-index oxides darkest, similar to earlier findings of scattering near-field microscopy at optical and infrared frequencies.[12,23] This near-field contrast can be again explained by dipolar near-field coupling between tip and sample which predicts higher signals s_2 for materials with higher dielectric values.

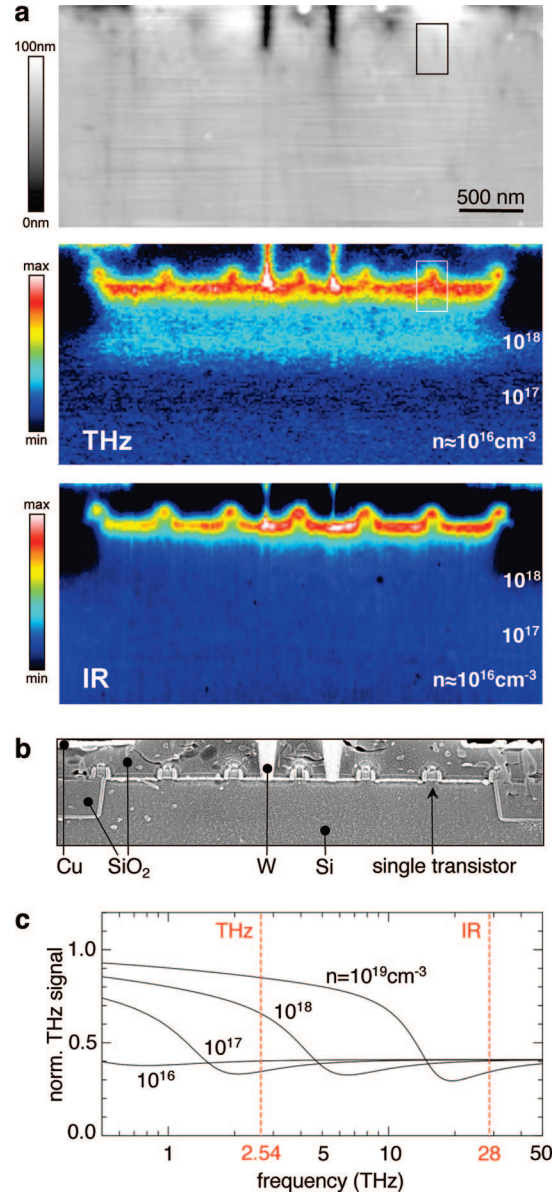

Figure 3. THz near-field microscopy of a polished cut through a multiple-transistor device structure. (a) AFM topography (gray) and simultaneously acquired THz near-field image s_2. The varying THz signal within the Si substrate reveals the different mobile carrier concentrations n indicated by numbers obtained from device simulations. The infrared near-field image s_2 ($\lambda \approx 11$ μm; taken for comparison) clearly demonstrates that only with THz illumination the varying mobile carrier concentration can be recognized. (b) The SEM image of a similar but decoration-etched sample validates that the THz image distinguishes different materials and the single transistors. The rectangle marks the zoom-in area depicted in Figure 4b,c. (c) THz signal amplitude s_2 calculated for n-doped Si as a function of the illumination frequency.

Near-field microscopy at THz frequencies particularly enables us to recognize mobile carriers and their distributions, in a concentration range centrally important for semiconductor science and technology ($n = 10^{16}-10^{19}$ carriers/cm^3) where visible and infrared methods lack sensitivity. This sensitivity can be clearly seen from the strong THz signal variations within the Si substrate of the device structure shown in Figure 3a. We observe a decreasing THz signal just below the transistors and a local maximum at 500 nm

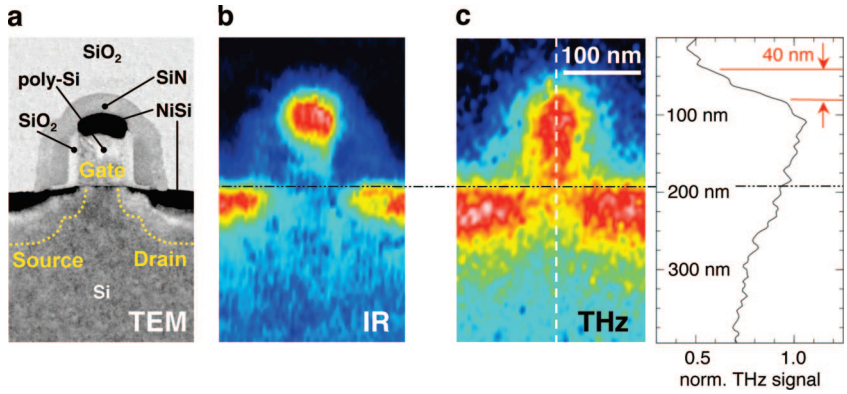

Figure 4. (a) TEM image of a single transistor. The highly doped regions below the source and drain NiSi contacts are marked by dashed yellow lines. (b) Infrared image s_3 of the single transistor marked in Figure 3a ($\lambda \approx 11$ μm). (c) High-resolution THz image s_3 of the single transistor marked in Figure 3a showing all essential parts of the transistor: source, drain and gate. The THz profile extracted along the dashed white line (averaged over a width of 12 nm and normalized to the signal obtained on the metallic NiSi gate contact) allows the estimation of a spatial resolution of about 40 nm, from the strong signal change at the SiO_2/SiN/NiSi transition.

depth. After passing a second minimum at about 900 nm depth, the THz signal reaches a constant level on intrinsically doped Si. A comparison with the nominal mobile carrier concentrations (the numbers in Figure 3a are from device simulations) provides clear evidence that the THz contrast maps the mobile carrier distribution with nanoscale resolution. For comparison we also show an infrared near-field image taken with a CO_2 laser at $\lambda \approx 11$ μm. It does not exhibit signal variations below the transistors. To explain the THz contrast in the theoretical framework mentioned above, we calculate the frequency-dependent THz signal s_2 (Figure 3c), between a metallic sphere and an extended Si surface where the mobile carrier response is described by a Drude term which depends on the mobile carrier concentration n.[24,25] The calculated spectra have highest THz signals at low frequencies and a shape which can be assigned to the near-field coupling between the tip and the mobile carrier plasmons in the Si sample. With increasing n, the spectral signature shifts to higher frequencies. Interestingly, a minimum near the plasma frequency is predicted, which occurs at 2.54 THz (red line in Figure 3c) for $n \approx 2 \times 10^{17}$ cm^{-3}. A minimum is indeed observed in the THz image (Figure 3a) at a depth of 900 nm below the transistors where the designed concentration gradient assumes a value of $n \approx 2 \times 10^{17}$ cm^{-3}. This good agreement between design, experiment, and theory enables immediate applications of THz near-field microscopy in semiconductor science and technology. Owing to the distinct relation between THz-plasmons and carrier concentration, our results open the door to quantitative mobile carrier profiling at the nanometer scale. This capability could be augmented by improving the model and by employing broadband THz spectroscopy.[26]

We provide first evidence of nanoscale resolved THz near-field microscopy by scanning a single transistor (marked in Figure 3a) at reduced pixel size (Figure 4). The comparison between a transmission electron microscopy image (TEM, Figure 4a), a near-field infrared image (Figure 4b) and a high-resolution THz image clearly verifies the capability of THz near-field microscopy to map the basic entities of the transistor: source, drain and gate (Figure 4c). In accordance with Figure 2 and dipolar coupling theory, the metallic NiSi parts exhibit higher near-field signals than the oxide and the weakly doped Si areas in both the IR and THz image. We quantify the exceptional high spatial resolution by extracting a THz line profile along the dashed white line showing a sharp signal increase from the low-refractive-index material SiO_2 to the metallic NiSi gate contact. Due to the smooth sample surface (see Figure 3a), we can exclude any topography-related artifact and also prove the pure dielectric origin of the THz contrast. This allows us to unambiguously determine a near-field optical resolution of about 40 nm (λ/3000).

In contrast to the IR image (Figure 4b), the THz image also reveals the highly doped poly-Si gate ($n \approx 10^{19}$ cm^{-3}) and the highly doped Si regions ($n \approx 10^{19}$ cm^{-3}) just below the metallic NiSi source and drain contacts. The THz signals here reach almost the values of the metal contacts, in good agreement with our prediction in Figure 3c. Furthermore, we find that between the NiSi source and drain contacts (black parts in the TEM image) the THz signal level reaches an intermediate value. According to our calculation in Figure 3c, this indicates a mobile carrier concentration in the order of 10^{18} cm^{-3} which is in good agreement with results from device simulations. Obviously, THz near-field microscopy allows for probing of mobile carriers in the 65 nm wide region between source and drain. In combination with future spectroscopic extensions,[8−10,13,26−28] this possibility could open the door to even measure the carrier mobility in this most important part of nanoscale semiconductor devices. Further applications include fundamental studies of mobile carrier properties in nanowires or nanoparticles.

An intriguing consequence follows from the sensitivity of our setup to mobile carrier concentrations in the range $10^{17}-10^{18}$ cm^{-3}, evident from the THz contrast shown in Figure 3a. Since the spatial resolution of 40 nm infers[20] that the volume probed by the THz near-field is about (40 nm)^3, we conclude that an average of less than 100 electrons in the probed volume suffices to evoke significant THz contrast. This opens the fascinating perspective that straightforward improvements of the current setup could master THz studies

of single electrons, and in conjunction with ultrafast techniques even their dynamics. Moreover, THz near-field microscopy seems predestined to study also other charged particles and quasiparticles in condensed matter, for example, in superconductors, low-dimensional electron systems, or conducting biopolymers, which possess intrinsic excitations at THz quantum energies and thus should exhibit resonantly enhanced THz contrast.

Note Added in Proof: Concerning novel THz probes, two further contributions have been published recently.[29,30]

Acknowledgment. Financially supported by BMBF within the NanoFutur program, Grant 03N8705, Deutsche Forschungsgemeinschaft Clusters of Excellence "Nanosystems Initiative Munich (NIM)" and "Munich-Centre for Advanced Photonics (MAP)", and Etortek project from the Government of the Basque Country. Angela Collantes (Infineon) is acknowledged for TEM imaging.

References

(1) Kuzmany, H. *Solid-State Spectroscopy*; Springer: Berlin, 1998.
(2) Ferguson, B.; Zhang, X. C. *Nat. Mater.* **2002**, *1*, 26–33.
(3) Mittleman, D., *Sensing with Terahertz Radiation*; Springer: Berlin, 2003.
(4) Tonouchi, M. *Nature Photon.* **2007**, *1*, 97–105.
(5) Chan, W. L.; Deibel, J.; Mittleman, D. M. *Rep. Prog. Phys.* **2007**, *70*, 1325–1379.
(6) Withayachumnankul, W.; Png, G. M.; Yin, X. X.; Atakaramians, S.; Jones, I.; Lin, H. Y.; Ung, B. S. Y.; Balakrishnan, J.; Ng, B. W. H.; Ferguson, B.; Mickan, S. P.; Fischer, B. M.; Abbott, D. *Proc. IEEE* **2007**, *95*, 1528–1558.
(7) Matarrese, L. M.; Evenson, K. M. *Appl. Phys. Lett.* **1970**, *17*, 8–10.
(8) van der Valk, N. C. J.; Planken, P. C. M. *Appl. Phys. Lett.* **2002**, *81*, 1558–1560.
(9) Chen, H. T.; Kersting, R.; Cho, G. C. *Appl. Phys. Lett.* **2003**, *83*, 3009–3011.
(10) Chen, H. T.; Kraatz, S.; Cho, G. C.; Kersting, R. *Phys. Rev. Lett.* **2004**, *93*, 267401.
(11) Planken, P. C. M.; van der Valk, N. C. J. *Opt. Lett.* **2004**, *29*, 2306–2308.
(12) Keilmann, F.; Hillenbrand, R. *Philos. Trans. R. Soc. London, Ser. A* **2004**, *362*, 787–805.
(13) Buersgens, F.; Kersting, R.; Chen, H. T. *Appl. Phys. Lett.* **2006**, *88*, 112115.
(14) Wang, K. L.; Mittleman, D. M.; van der Valk, N. C. J.; Planken, P. C. M. *Appl. Phys. Lett.* **2004**, *85*, 2715–2717.
(15) Maier, S. A.; Andrews, S. R.; Martin-Moreno, L.; Garcia-Vidal, F. J. *Phys. Rev. Lett.* **2006**, *97*, 176805.
(16) Novotny, L.; Sanchez, E. J.; Xie, X. S. *Ultramicroscopy* **1998**, *71*, 21–29.
(17) Cvitkovic, A.; Ocelic, N.; Aizpurua, J.; Guckenberger, R.; Hillenbrand, R. *Phys. Rev. Lett.* **2006**, *97*, 60801.
(18) de Abajo, F. J. G.; Howie, A. *Phys. Rev. Lett.* **1998**, *80*, 5180–5183.
(19) de Abajo, F. J. G.; Howie, A. *Phys. Rev. B* **2002**, *65*, 115418.
(20) Novotny, L.; Hecht, B. *Principles of Nano-Optics*; Cambridge University Press: Cambridge, 2007.
(21) Ocelic, N.; Huber, A.; Hillenbrand, R. *Appl. Phys. Lett.* **2006**, *89*, 101124.
(22) Buersgens, F.; Acuna, G.; Lang, C. H.; Potrebic, S. I.; Manus, S.; Kersting, R. *Rev. Sci. Instrum.* **2007**, *78*, 113701.
(23) Taubner, T.; Hillenbrand, R.; Keilmann, F. *J. Microsc. (Oxford)* **2003**, *210*, 311–314.
(24) Huber, A. J.; Kazantsev, D.; Keilmann, F.; Wittborn, J.; Hillenbrand, R. *Adv. Mater.* **2007**, *19*, 2209–2212.
(25) Knoll, B.; Keilmann, F. *Appl. Phys. Lett.* **2000**, *77*, 3980–3982.
(26) von Ribbeck, H. G.; Brehm, M.; van der Weide, D. W.; Winnerl, S.; Drachenko, O.; Helm, M.; Keilmann, F. *Opt. Express* **2008**, *16*, 3430–3438.
(27) Zhan, H.; Astley, V.; Hvasta, M.; Deibel, J. A.; Mittleman, D. M.; Lim, Y. S. *Appl. Phys. Lett.* **2007**, *91*, 162110.
(28) Naftaly, M.; Miles, R. E. *Proc. IEEE* **2007**, *95*, 1658–1665.
(29) Kawano, Y.; Ishibashi, K. *Nature Photon.* **2008**, doi: 10.1038/nphoton2008.157.
(30) Rusina, A.; Durach, M.; Nelson, K. A.; Stockman, M. I. **2008**, arXiv:0808.1324.

NL802086X